

# Ab initio thermodynamic results for the degenerate electron gas at finite temperature

T. Schoof, S. Groth, J. Vorberger, and M. Bonitz

*Institut für Theoretische Physik und Astrophysik,*

*Christian-Albrechts-Universität zu Kiel, D-24098 Kiel, Germany*

(Dated: December 3, 2024)

The uniform electron gas (UEG) at finite temperature is of key relevance for many applications in dense plasmas, warm dense matter, laser excited solids and much more. Accurate thermodynamic data for the UEG are an essential ingredient for many-body theories, in particular, density functional theory. Recently, first-principle restricted path integral Monte Carlo results became available which, however, due to the fermion sign problem, had to be restricted to moderate degeneracy, i.e. low to moderate densities with  $r_s = \bar{r}/a_B \gtrsim 1$ . Here we present novel first-principle configuration PIMC results for polarized electrons for  $r_s \leq 1$ . We also present quantum statistical data within the  $e^4$ -approximation that are in good agreement with the simulations at small to moderate  $r_s$ .

PACS numbers: 05.30-d, 05.30.Fk, 71.10.Ca

Thermodynamic properties of quantum degenerate electrons are vital for the description of matter at high densities, e.g. [1–3], such as dense plasmas in compact stars or planet cores, e.g. [4–6], as well as in laser fusion experiments at NIF, e.g. [7–9], Rochester [10] or Sandia [11, 12]. Besides, the electron component is of crucial importance for understanding the properties of atoms, molecules and existing and novel materials. The most successful approach has been density functional theory (DFT)-combined with an approximation for the exchange-correlation potential. Its success is based on the availability of accurate *zero temperature* data for the UEG which is obtained from analytically known limiting cases combined with first-principle quantum Monte Carlo data [13].

In recent years more and more applications have emerged where the electrons are highly excited, e.g. by compression of the material or by electromagnetic radiation (see above), which require to go beyond zero temperature DFT. This has led to an urgent need for accurate thermodynamic data of the UEG at *finite temperature*. One known limiting case is the highly degenerate ideal Fermi gas (IFG), and perturbation theory results around the IFG, starting with the Hartree-Fock and first order correlation corrections (Montroll-Ward) [14, 15], are long known; for an analytical fit at high densities, see Ref. [16] and for further improved approximations, such as the  $e^4$ -approximation, see Refs. [17–19]. These approximations break down when the Coulomb interaction energy among the electrons becomes comparable to their kinetic energy, requiring computer simulations such as path integral Monte Carlo (PIMC), e.g. [20]. While restricted PIMC (RPIMC) results for dense multi-component quantum plasmas, e.g. [21, 22] as well as direct fermionic PIMC (DPIMC) results [23–26] have been available already for 15 years, only recently finite temperature RPIMC results for the UEG (or helium) have been obtained [27]. It is well known that fermionic PIMC simulation in continuous space suffer the fermion sign problem (FSP) which is known to be NP hard [28]. This means, with increasing quantum degen-

eracy, i.e. increasing parameter  $\chi = n\lambda_{DB}^3$ , which is the product of density and thermal DeBroglie wave length,  $\lambda_{DB}^2 = h^2[2\pi m k_B T]^{-1}$ , the simulations suffer an exponential loss of accuracy. RPIMC formally avoids the FSP by an additional assumption on the nodes of the density matrix, however, it also cannot access high densities [29],  $r_s < 1$  [ $r_s = \bar{r}/a_B$ , where  $\bar{r}$  is the mean interparticle distance,  $n^{-1} = 4\pi\bar{r}^3/3$  and  $a_B$  the Bohr radius]. Also, the quality of the simulations around  $r_s = 1$ , at low temperatures  $\Theta = k_B T/E_F \leq 0.125$  [ $E_F$  is the Fermi energy] is unknown. However, this leaves out the high-density range that is of high importance, e.g. for deuterium-tritium implosions at NIF where mass densities of  $400 \text{ gcm}^{-3}$  (up to  $1596 \text{ gcm}^{-3}$ ) have recently been reported [9] (are expected along the implosion path [8]), corresponding to  $r_s \approx 0.24$  ( $r_s = 0.15$ ), see Fig. 1.

The authors of Ref. [27] also performed DPIMC simulations which confirmed that, for  $\Theta < 0.5$  and  $r_s \lesssim 4$ , these simulations are practically not possible, see Fig. 1. We also mention independent recent DPIMC simulations [30] that are overall in good agreement with the data of Ref. [27] but indicate large deviations for the lowest temperatures and  $r_s \lesssim 2$  (the energies are lower). Finally, a recent attempt to avoid the FSP by an approximate treatment of exchange cycles [31] also yielded lower energies for  $r_s = 1$  and  $\Theta = 0.125$  than the RPIMC data of Ref. [27]. To bridge the gap between the known analytical result for the ideal Fermi gas at  $r_s = 0$  and previous simulations ( $r_s \gtrsim 1$ ) and to provide comprehensive input data for finite temperature DFT, several fits have been proposed recently [32, 33]. However, they naturally depend to a high degree on the quality of the simulation data upon which they are based.

It is the purpose of this Letter to improve this situation. We present the first ab initio simulation results that avoid a simplified treatment of fermionic exchange for  $r_s \lesssim 1$  and finite temperatures,  $\Theta \lesssim 0.5$ . We apply the recently developed fermionic configuration path integral Monte Carlo (CPIMC) approach to the UEG and demonstrate its capabilities for 33 spin polarized electrons in a cubic box of side length  $L$  (as was studied

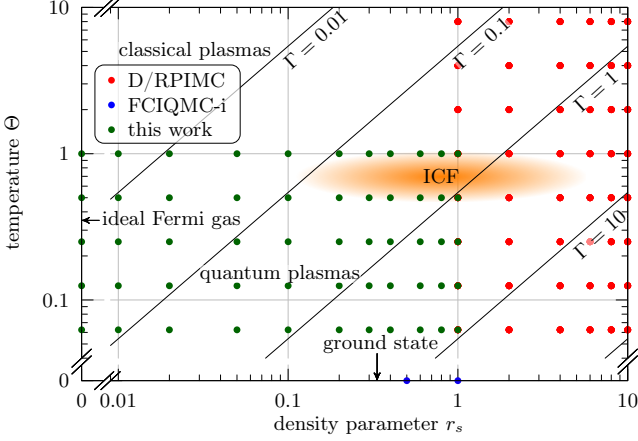


FIG. 1: Density-temperature plain in the warm dense matter range. ICF: typical inertial confinement fusion parameters [8]. Quantum (classical) behavior dominates below (above) the line  $\Theta = 1$ .  $\Gamma = e^2/\bar{r}k_B T$  is the classical coupling parameter. Red dots: available finite temperature RPIMC [27] and DPIMC [30] data for the UEG. Blue dots: ground state data of Ref. [38]. Green dots: CPIMC and analytical results of this work.

in [31, 33]). Our simulations have no sign problem for  $0 \leq r_s \leq 0.4$  and yield accurate thermodynamic data up to  $r_s = 1$ .

**CPIMC for the UEG.** The jellium Hamiltonian in second quantization with respect to plane waves  $\langle \vec{r} | \vec{k} \rangle = \frac{1}{L^{3/2}} e^{i\vec{k} \cdot \vec{r}}$  with  $\vec{k} = \frac{2\pi}{L} \vec{m}$ ,  $\vec{m} \in \mathbb{Z}^3$  has the familiar form (we use Rydberg units throughout)

$$\hat{H} = \sum_i \vec{k}_i^2 \hat{a}_{\vec{k}_i}^\dagger \hat{a}_{\vec{k}_i} + 2 \sum_{\substack{i < j, k < l \\ i \neq k, j \neq l}} w_{ijkl}^- \hat{a}_i^\dagger \hat{a}_j^\dagger \hat{a}_l \hat{a}_k + E_M, \quad (1)$$

$$w_{ijkl}^- = w_{ijkl} - w_{ijlk}, \quad w_{ijkl} = \frac{4\pi e^2}{L^3} \frac{\delta_{\vec{k}_i + \vec{k}_j, \vec{k}_k + \vec{k}_l}}{\vec{k}_{ik}^2}, \quad (2)$$

where the first (second) term describes the kinetic (interaction) energy, and  $\vec{k}_{ik} = \vec{k}_i - \vec{k}_k$ . The Madelung energy  $E_M$  accounts for the self-interaction of the Ewald summation in periodic boundary conditions [34] for which we found  $E_M \approx -2.837297 \cdot (3/4\pi)^{\frac{1}{3}} N^{\frac{2}{3}} r_s^{-1}$ . The operator  $\hat{a}_i^\dagger$  ( $\hat{a}_i$ ) creates (annihilates) a particle in the orbital  $|\vec{k}_i\rangle$ . In the interaction term, the  $\vec{k}_i = \vec{k}_k$  and  $\vec{k}_j = \vec{k}_l$  components cancel with the interactions with the positive background. While the complete (infinite) set of plane waves  $\langle \vec{r} | \vec{k}_i \rangle$  forms a basis in the single-particle Hilbert space, for practical simulations it has to be truncated at a total number  $N_B$  of orbitals.

In conventional RPIMC and DPIMC, the system (1) is treated in the coordinate representation allowing for a numerically exact description in the classical strongly coupled limit and for weak degeneracy. CPIMC [35], in contrast, is constructed in a way that it allows for exact simulations in the opposite limit of the ideal Fermi

gas,  $r_s = 0$  [36], and at weak to moderate coupling and strong degeneracy. This is achieved by representing the  $N$ -electron state in second quantization [37] as  $|\{n\}\rangle = |n_1, n_2, \dots\rangle$ , where the  $n_i$  are fermionic occupation numbers ( $n_i = 0, 1$ ) of the single-particle orbitals  $|\vec{k}_i\rangle$ . This way, fermionic anti-symmetry is “built in” exactly into the states. The partition function  $Z$  and quantum-statistical expectation values, such as the internal energy  $U$ , are straightforwardly computed in Fock space as

$$Z(\Theta, r_s; N) = \text{Tr}_{|\{n\}\rangle} e^{-\beta \hat{H}}, \quad (3)$$

$$U(\Theta, r_s; N) = \langle \hat{H} \rangle = \text{Tr}_{|\{n\}\rangle} \hat{H} \frac{e^{-\beta \hat{H}}}{Z}, \quad (4)$$

avoiding the sum over  $N!$  permutations over the canonical density operator  $e^{-\beta \hat{H}}$  that is the origin of the notorious FSP in DPIMC. The trace is evaluated using the concept of continuous time path integral Monte Carlo which has been successfully applied to bosonic lattice models [40–43]. We have generalized this concept to continuous fermionic systems with long range interactions [35, 44]. The main idea is to split the Hamiltonian into a diagonal,  $\hat{D}$ , and an off-diagonal part,  $\hat{Y}$  and summing up the entire perturbation series of the density operator  $e^{-\beta \hat{H}}$  in terms of  $\hat{Y}$ . The final result, for the case of the UEG, is [45]:

$$Z = \sum_{\substack{K=0, \\ K \neq 1}}^{\infty} \sum_{\{n\}} \sum_{s_1 \dots s_{K-1}} \int_0^{\beta} d\tau_1 \int_{\tau_1}^{\beta} d\tau_2 \dots \int_{\tau_{K-1}}^{\beta} d\tau_K \quad (5)$$

$$(-1)^K e^{-\sum_{i=0}^K D_{\{n^{(i)}\}}(\tau_{i+1} - \tau_i)} \prod_{i=1}^K (-1)^{\alpha_{s_i}} w_{s_i}^-,$$

$$D_{\{n^{(i)}\}} = \sum_l \vec{k}_l^2 n_l^{(i)} + \sum_{l < k} w_{lklk}^- n_l^{(i)} n_k^{(i)}, \quad (6)$$

$$\alpha_{s_i} = \alpha_{pqrs}^{(i)} = \sum_{l=p}^{q-1} n_l^{(i-1)} + \sum_{l=r}^{s-1} n_l^{(i)}.$$

where  $s_i = \{(p, q, r, s), \quad p < q, \quad r < s\}$ , denotes a quadruple of orbital indices.

Thus the partition function is represented as a sum over  $\beta$ -periodic “paths” in Fock space, in imaginary time, which we illustrate in Fig. 2: For an ideal Fermi system a path is characterized by a single  $N$ -particle Slater determinant  $|\{n\}\rangle$ . For a correlated Fermi system the original determinant  $|\{n\}\rangle = |\{n^{(0)}\}\rangle$  (straight horizontal lines in Fig. 2) is interrupted by excitations of the type  $(s, \tau)$ : at time  $\tau$ , a pair of occupied orbitals  $|\vec{k}_r\rangle, |\vec{k}_s\rangle$  is replaced by the previously empty pair  $|\vec{k}_p\rangle, |\vec{k}_q\rangle$ . Paths differ by the number  $K$  of excitations (“kinks”), their times  $\tau_1 \dots \tau_k$  on the  $\tau$ -interval  $[0, \beta]$  and the involved quadruples of orbitals  $s_1 \dots s_K$ . The partition function clearly reflects this summation over the different types of kinks, integration over the kink times and summation over  $K$  [cf. first

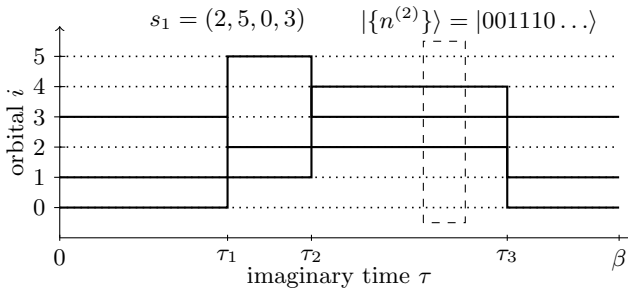


FIG. 2: Typical closed path in Slater determinant (Fock) space. The state with three occupied orbitals  $|\vec{k}_0\rangle, |\vec{k}_1\rangle, |\vec{k}_3\rangle$  undergoes a two-particle excitation  $(s_1, \tau_1)$  that replaces the occupied orbitals  $|\vec{k}_0\rangle, |\vec{k}_3\rangle$  by  $|\vec{k}_2\rangle, |\vec{k}_5\rangle$ . Two further excitations occur at  $\tau_2$  and  $\tau_3$ . The states at the “imaginary times”  $\tau = 0$  and  $\tau = \beta$  coincide. All possible paths contribute to the partition function  $Z$ , Eq. (5).

line of Eq. (5)]. The weight of each path [terms in the second line of Eq. (5)] is determined by the Fock state matrix elements of the Hamiltonian, where diagonal elements  $D_{\{n^{(i)}\}}$ , Eq. (6), arise from the kinetic energy and the mean-field part of the Coulomb interaction, whereas off-diagonal elements,  $(-1)^{\alpha_{s_i}} w_{s_i}^-$ , are due to the remaining Coulomb interaction (correlation part) [46]. We underline that expression (5) is exact for  $N_B \rightarrow \infty$  and, thus, allows for ab initio thermodynamic simulations of the UEG.

Formula (5) and similar expressions for thermodynamic observables, such as the internal energy [45], can be efficiently evaluated using Metropolis Monte Carlo. To this end, we developed an algorithm that generates all possible paths in Slater determinant space thereby assuring ergodicity. For the UEG a total of 6 different steps are required, including addition and removal of a single kink and pairs of kinks, modification of an existing kink and excitation of single orbitals. The complete set of steps and the associated MC algorithm cannot be presented here, for details see Ref. [45].

**Numerical results.** Our finite-temperature CPIMC algorithm was extensively tested for Coulomb interacting fermions in a 1D harmonic oscillator [35]. A first test of the present algorithm for the UEG for  $N = 4$  particles showed excellent agreement with exact diagonalization results [45]. Here, we extend these simulations to  $N = 33$  particles. First we check the convergence with respect to the single-particle basis dimension  $N_B$  and show a typical case in Fig. 3.a, for  $r_s = 0.4$  and four temperatures. The scaling with respect to  $x = 1/N_B$  allows for a reliable extrapolation to  $x \rightarrow 0$  and to set the basis size to  $N_B = 2109$  that was used in all simulations, giving a relative basis incompleteness error not exceeding the statistical error ( $1\sigma$  standard deviation).

With these parameters, we have performed extensive CPIMC simulations in a broad range of  $r_s$ - and  $\Theta$ -values. In contrast to DPIMC and RPIMC, our ab initio simu-

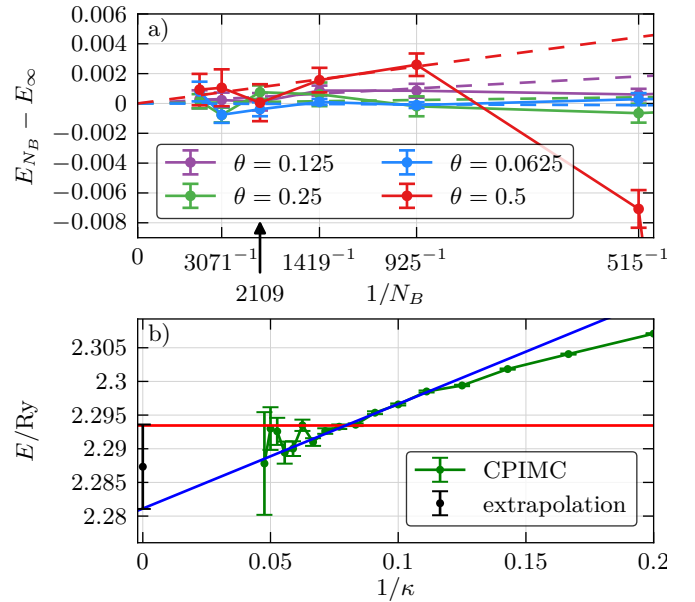


FIG. 3: Convergence of the CPIMC simulations. **a.** Convergence with the single-particle basis size  $N_B$  for  $r_s = 0.4$ . **b.** Convergence with respect to the kink potential parameter  $\kappa$  (see text) and extrapolation to  $1/\kappa \rightarrow 0$ , corresponding to  $K \rightarrow \infty$ , for  $r_s = 1.0$  and  $\theta = 0.0625$ . The asymptotic value is enclosed between the red and blue line.

lations (without any simplifications besides the choice of  $N_B$ ) pose no problem for the ideal and weakly coupled UEG, up to  $r_s \sim 0.4$ . For larger  $r_s$ , we observe a rapid decrease of the average sign, in analogy to the harmonic oscillator case [35]. This gives rise to convergence problems of the MC algorithm in case a path with many kinks is attempted. We, therefore, introduce an artificial kink potential in Eq. (5),  $V_\kappa(K) = [e^{-(\kappa+0.5-K)} + 1]^{-1}$ , for calculations with  $r_s > 0.4$ , yielding the correct partition function in the limit  $\kappa \rightarrow \infty$ . Performing simulations for different  $\kappa$ , we generally observe a rapid convergence of the total energy allowing for an extrapolation to  $1/\kappa \rightarrow 0$ . This is demonstrated for the most difficult case ( $r_s = 1, \Theta = 0.0625$ ) in Fig. 3.b. The asymptotic value and the error estimate are computed from the two extreme cases of a horizontal and linear extrapolation. With this procedure the simulations could be extended to  $r_s = 1$ , with the total error not exceeding 0.3%.

Our simulation results for the exchange-correlation energy  $E_{xc}$  are summarized in Fig. 4. The data cover the whole density range from  $r_s = 0$  to  $r_s = 1$ , including the ideal Fermi gas limit where  $E_{xc}r_s \rightarrow \text{const}$ , approaching the Hartree-Fock limit. A detailed table of the various energy contributions is presented in the supplementary material [48]. An interesting observation is the non-monotonic dependence on temperature (cf. the crossing of the red and pink curves) which is also observed in RPIMC and in the macroscopic data of Karasiev *et al.* [32]. Interestingly, all curves seem to cross over smoothly into the RPIMC data [27, 47] for the same con-

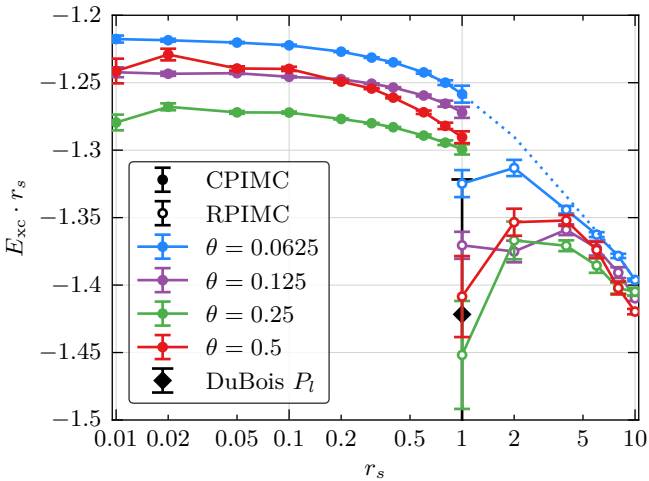


FIG. 4: (Color online) Exchange-correlation energy (times  $r_s$ ) for 33 spin-polarized electrons and four temperatures. Comparison of our CPIMC results (full symbols with error bars [49]) and RPIMC results of Ref. [27] (open symbols). The dotted line is an interpolation between the CPIMC and RPIMC data for  $\Theta = 0.0625$ . Also shown is the data point of DuBois *et al.* [31] for  $\Theta = 0.125$ .

ditions, for  $r_s \gtrsim 4$ , as indicated by the dotted line. There is an obvious mismatch in the range  $r_s \sim 1 \dots 4$ . Since our curves are accurate within the given error, this discrepancy is expected to be due to the (unknown) systematic error involved in RPIMC. Also, the energy obtained within the novel approach of DuBois *et al.* [31], cf. the data point for  $r_s = 1$  and  $\Theta = 0.125$  in Fig. 4, is found to be too low.

**Macroscopic results.** Predictions for a macroscopic system, based on data for just 33 particles, will inevitably lead to a loss of accuracy. Brown *et al.* have attempted such a mapping of their RPIMC data for  $N = 33$  to  $N \rightarrow \infty$  and published finite size corrections [FSC (a)] in the supplement of Ref. [27]. A ground state formula [FSC (b)] has been presented by Drummond *et al.* [50]. Both FSC deviate significantly from each other, so we tested both and show the results in Fig. 5 and in [48]. Version (b) yields, for  $\Theta = 0.0625$ , macroscopic data [points CPIMC (b)] that are in very good agreement with analytical approximations (see below), in the range  $0.8 \lesssim r_s \lesssim 1$ , and smoothly connect to the RPIMC data, for  $r_s \gtrsim 4$ . For higher densities the formula is not applicable. For higher temperature, cf. data for  $\Theta = 0.5$ , the ground state FSC (b) is too small and we applied a Sommerfeld correction [48]. In contrast, the FSC of Brown [points CPIMC (a)] produces energies that are substantially too large and have to be discarded.

To obtain independent analytical results for the macroscopic UEG, we now compute the exchange correlation energy including, in addition to Hartree-Fock [32], the two second order diagrams (Montroll Ward and  $e^4$ ) [48]. The two results [cf. Fig. 5], converge for low  $r_s$ , eventually reaching the Hartree-Fock asymptote (horizontal

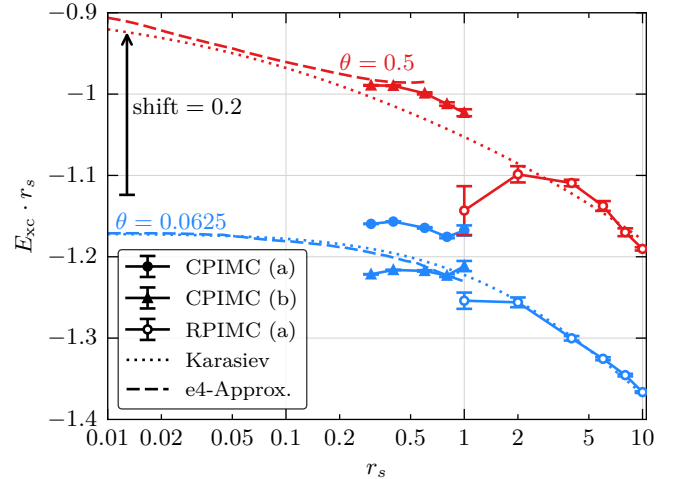


FIG. 5: (Color online) Exchange correlation energy (times  $r_s$ ) of the macroscopic polarized UEG at  $\Theta = 0.0625$  (blue) and  $\Theta = 0.5$  (red). Open symbols: RPIMC results [27]. CPIMC (b): our results with FSC from Refs. [50, 51]. CPIMC (a): our data with the FSC from Ref. [27]. Dashes: analytical  $e^4$ -approximation [48], dots: fit of Ref. [32]. For better visibility the curves for  $\Theta = 0.5$  are upshifted by 0.2.

line). For  $r_s \gtrsim 0.1$ , MW and  $e^4$  start to deviate from one another, and we expect the exact result to be enclosed between the two [48]. Reliable predictions are possible up to  $r_s \sim 0.8$ , for  $\Theta = 0.0625$ , and  $r_s \sim 0.55$ , for  $\Theta = 0.5$  [48]. In Figure 5 we also include the fit of Ref. [32] that shows, overall, a very good behavior, but is too low at  $r_s \rightarrow 0$ , with the deviations growing with  $\Theta$  [48].

To summarize, we have presented first-principle configuration PIMC results for the UEG at finite temperature that have no sign problem at high quantum degeneracy,  $r_s \lesssim 0.4$ , and allow for reliable predictions up to  $r_s = 1$ . This makes CPIMC a perfect complementary approach to direct fermionic PIMC and to RPIMC that cannot access high densities. Our results indicate that the previous RPIMC data are not reliable in the range  $r_s \lesssim 4$ , and our data constitute a valuable benchmark for improved simulations. Furthermore, our accurate analytical results for small  $r_s$  will allow to improve the fit of Ref. [32]. The present results will be important for dense quantum plasmas at finite temperatures, that are relevant for warm dense matter, in general, and for ICF, in particular. Furthermore, the obtained accurate results for the exchange-correlation energy provide benchmark results for finite temperature DFT simulations. Although the fermion sign problem is not removed by our approach, the proposed combination of CPIMC with DPIMC (or RPIMC) provides, for the UEG, a practical way around this problem.

We acknowledge stimulating discussions with V. Filinov, J.W. Dufty, V.V. Karasiev and S. Trickey and E. Brown for providing information on the FSC (a) used in Ref. [27]. This work is supported by the Deutsche Forschungsgemeinschaft via grant BO1366/10 and by

grant SHP006 for supercomputing time at the HLRN.

---

[1] L.B. Fletcher *et al.*, *Observations of Continuum Depression in Warm Dense Matter with X-Ray Thomson Scattering*, *Phys. Rev. Lett.* **112**, 145004 (2014).

[2] D. Kraus *et al.*, *Probing the Complex Ion Structure in Liquid Carbon at 100 GPa*, *Phys. Rev. Lett.* **111**, 255501 (2013).

[3] S. Regan *et al.*, *Inelastic X-Ray Scattering from Shocked Liquid Deuterium*, *Phys. Rev. Lett.* **109**, 265003 (2012).

[4] M.D. Knudson *et al.*, *Probing the Interiors of the Ice Giants: Shock Compression of Water to 700 GPa and 3.8g/cm<sup>3</sup>*, *Rev. Lett.* **108**, 091102 (2012).

[5] B. Militzer, W.B. Hubbard, J. Vorberger, I. Tamblyn, and S.A. Bonev, *A Massive Core in Jupiter Predicted from First-Principles Simulations*, *Astrophys J.* **688**, L45, (2008).

[6] N. Nettelmann, A. Becker, B. Holst, and R. Redmer, *Jupiter Models with Improved Ab Initio Hydrogen Equation of State (H-REOS.2)*, *Astrophys. J.* **750**, 52 (2012).

[7] J. D. Lindl *et al.* *The physics basis for ignition using indirect-drive targets on the National Ignition Facility*, *Phys. Plasmas* **11**, 339 (2004).

[8] S.X. Hu, B. Militzer, V.N. Goncharov, and S. Skupsky, *First-principles equation-of-state table of deuterium for inertial confinement fusion applications*, *Phys. Rev. B* **84**, 224109 (2011).

[9] O. Hurricane *et al.*, *Fuel gain exceeding unity in an inertially confined fusion implosion*, *Nature* **506**, 343 (2014).

[10] R. Nora *et al.*, *Gigabar Spherical Shock Generation on the OMEGA Laser*, *Phys. Rev. Lett.* **114**, 045001 (2015).

[11] M.R. Gomez *et al.*, *Experimental Demonstration of Fusion-Relevant Conditions in Magnetized Liner Inertial Fusion*, *Phys. Rev. Lett.* **113**, 155003 (2014).

[12] P.F. Schmidt *et al.*, *Understanding Fuel Magnetization and Mix Using Secondary Nuclear Reactions in Magnetohydrodynamic Inertial Fusion*, *Phys. Rev. Lett.* **113**, 155004 (2014).

[13] D.M. Ceperley, B.J. Alder, *Ground State of the Electron Gas by a Stochastic Method*, *Phys. Rev. Lett.* **45**, 566 (1980).

[14] H.E. DeWitt, *Thermodynamic Functions of a partially degenerate fully ionized gas*, *J. Nucl. Energy C* **2**, 27–45 (1961).

[15] W.D. Kraeft, and W. Stolzmann, *Thermodynamic functions of Coulomb systems*, *Physica A* **97**, 306 (1979).

[16] F. Perrot and M.W.C. Dharma-wardana, *Exchange and correlation potentials for electron-ion systems at finite temperatures*, *Phys. Rev. A* **30**, 2619 (1984).

[17] W.D. Kraeft, D. Kremp, W. Ebeling, and G. Röpke, *Quantum Statistics of Charged Particle Systems*, Akademie-Verlag, Berlin 1986.

[18] D. Kremp, M. Schlanges, and W.D. Kraeft, *Quantum Statistics of Nonideal Plasmas*, Springer (2005).

[19] J. Vorberger, M. Schlanges, W.-D. Kraeft, *Equation of state for weakly coupled quantum plasmas*, *Phys. Rev. E* **69**, 046407 (2004).

[20] D.M. Ceperley, *Path integrals in the theory of condensed helium*, *Rev. Mod. Phys.* **65**, 279 (1995).

[21] B. Militzer, and R. Pollock, *Variational density matrix method for warm, condensed matter: Application to dense hydrogen*, *Phys. Rev. E* **61**, 3470 (2000).

[22] B. Militzer, *First Principles Calculations of Shock Compressed Fluid Helium*, *Phys. Rev. Lett.* **97** (2006) 175501.

[23] V.S. Filinov, M. Bonitz, and V.E. Fortov, *High density phenomena in hydrogen plasma*, *JETP Letters* **72**, 245 (2000).

[24] V.S. Filinov, M. Bonitz, W. Ebeling, and V.E. Fortov, *Thermodynamics of hot dense H-plasmas: Path integral Monte Carlo simulations and analytical approximations*, *Plasma Phys. Control. Fusion* **43**, 743 (2001).

[25] A. Filinov, V. Golubnychiy, M. Bonitz, W. Ebeling, and J.W. Dufty, *Temperature-dependent quantum pair potentials and their application to dense partially ionized hydrogen plasmas*, *Phys. Rev. E* **70**, 046411 (2004).

[26] M. Bonitz, V. S. Filinov, V. E. Fortov, P. R. Levashev, and H. Fehske, *Crystallization in Two-Component Coulomb Systems*, *Phys. Rev. Lett.* **95**, 235006 (2005).

[27] E.W. Brown, B. K. Clark, J. L. DuBois, and D. M. Ceperley, *Path-Integral Monte Carlo Simulation of the Warm Dense Homogeneous Electron Gas*, *Phys. Rev. Lett.* **110**, 146405 (2013).

[28] M. Troyer, and U.-J. Wiese, *Computational complexity and fundamental limitations to fermionic quantum Monte Carlo simulations*, *Phys. Rev. Lett.* **94**, 170201 (2005).

[29] While RPIMC simulations avoid the fermion sign problem they fail to reproduce the ideal Fermi gas limit, as was shown by V. Filinov, *J. Phys. A: Math. Gen.* **34**, 1665 (2001) and *High Temperature* **52**, 615 (2014).

[30] V.S. Filinov, M. Bonitz, Zh. Moldabekov, and V.E. Fortov, *Fermionic path integral Monte Carlo results for the uniform electron gas at finite temperature*, submitted for *Phys. Rev. E*, arxiv: 1407.3600.

[31] J.L. DuBois, B.J. Alder, and E.W. Brown, *Overcoming the fermion sign problem in homogeneous systems*, arXiv:1409.3262.

[32] V.V. Karasiev, T. Sjostrom, J. Dufty, and S. B. Trickey *Accurate Homogeneous Electron Gas Exchange-Correlation Free Energy for Local Spin-Density Calculations*, *Phys. Rev. Lett.* **112**, 076403 (2014) and Supplementary Material.

[33] E.W. Brown, J. L. DuBois, M. Holzmann, and D. M. Ceperley, *Exchange-correlation energy for the three-dimensional homogeneous electron gas at arbitrary temperature*, *Phys. Rev. B* **88**, 081102(R) (2013); **88**, 199901(E) (2013).

[34] L. M. Fraser and W. M. C. Foulkes, *Finite-size effects and Coulomb interactions in quantum Monte Carlo calculations for homogeneous systems with periodic boundary conditions*, *Phys. Rev. B* **53**, 1814 (1996).

[35] T. Schoof, M. Bonitz, A. Filinov, D. Hochstuhl, and J.W. Dufty, *Configuration Path integral Monte Carlo*, *Contrib. Plasma Phys.* **51**, 687 (2011).

[36] In this paper we restrict ourselves to the non-relativistic jellium model.

[37] This concept is also used in zero temperature full configuration Monte Carlo [38, 39].

[38] J.J. Shepherd, G.H. Gooth, A. Grüneis, and A. Alavi,

*Full configuration interaction perspective on the homogeneous electron gas*, Phys. Rev. B **85**, 081103(R) (2012).

[39] J.J. Shepherd, G.H. Gooth, and A. Alavi, *Investigation of the full configuration interaction quantum Monte Carlo method using homogeneous electron gas models*, J. Chem. Phys. **136**, 244101 (2012).

[40] N.V. Prokofev, B.V. Svistunov, and I.S. Tupitsyn, *Exact quantum Monte Carlo process for the statistics of discrete systems*, JETP Lett. **64**, 911 (1996) [Pisma Zh. Exp. Teor. Fiz. **64**, 853 (1996)].

[41] N.V. Prokofev, B.V. Svistunov, and I.S. Tupitsyn, *Exact, complete, and universal continuous-time worldline Monte Carlo approach to the statistics of discrete quantum systems*, JETP **87**, 310 (1998).

[42] K. Van Houcke, S.M.A. Rombouts, and L. Pollet, *Quantum Monte Carlo simulation in the canonical ensemble at finite temperature*, Phys. Rev. E **73**, 056703 (2006).

[43] S.M.A. Rombouts, K. Van Houcke and L. Pollet, *Loop Updates for Quantum Monte Carlo Simulations in the Canonical Ensemble*, Phys. Rev. Lett. **96**, 180603 (2006).

[44] S. Groth, T. Schoof, and M. Bonitz, Chapter in: *Complex Plasmas: Scientific Challenges and Technological Opportunities*, M. Bonitz, K. Becker, J. Lopez, and H. Thomsen (eds.), Springer 2014.

[45] T. Schoof, S. Groth, and M. Bonitz, *Towards ab Initio Thermodynamics of the Electron Gas at Strong Degeneracy*, Contrib. Plasma Phys. **55**, 136 (2015).

[46] Note that, due to momentum conservation, only two-particle excitations  $s_i$  are possible (for the general case, see Ref. [45]), and the restriction to closed paths requires  $K \neq 1$ .

[47] The RPIMC data for  $N = 33$  were obtained by applying, to the total energy results of Ref. [27], the finite size corrections given in the Supplement of that reference and, subtracting, in addition, the energy of the corresponding ideal 33-particle system.

[48] Supplementary material

[49] The fluctuations of  $E_{xc}$  at small  $r_s$  arise from the vanishing of the exchange-correlation energy, compared to the total energy, for  $r_s \rightarrow 0$ . While the total energy is well converged,  $E_{xc}$  retains a substantial relative error.

[50] N. D. Drummond, R. J. Needs, A. Sorouri, and W. M. C. Foulkes, *Finite-size errors in continuum quantum Monte Carlo calculations*, Phys. Rev. B **78**, 125106 (2008).

[51] To account for finite temperature effects we used the Drummond formula [50] with a Sommerfeld correction. Details are given in the supplementary material [48].